NANO LETTERS
Cite This: Nano Lett. 2019, 19, 6886−6893
Letter
pubs.acs.org/NanoLett

Direct Observation of Gate-Tunable Dark Trions in Monolayer WSe_2

Zhipeng Li,[†,¶] Tianmeng Wang,[†,¶] Zhengguang Lu,[‡,§] Mandeep Khatoniar,[◆,⊥] Zhen Lian,[†] Yuze Meng,[†] Mark Blei,[#] Takashi Taniguchi,[☆] Kenji Watanabe,[☆] Stephen A. McGill,[‡] Sefaattin Tongay,[#] Vinod M. Menon,[◆,⊥] Dmitry Smirnov,[‡] and Su-Fei Shi*[,†,▽]

[†]Department of Chemical and Biological Engineering, Rensselaer Polytechnic Institute, Troy, New York 12180, United States
[‡]National High Magnetic Field Lab, Tallahassee, Florida 32310, United States
[§]Department of Physics, Florida State University, Tallahassee, Florida 32306, United States
[◆]Department of Physics, City College of New York, City University of New York, 160 Convent Ave., New York, New York 10031, United States
[⊥]Department of Physics, The Graduate Center, City University of New York, 365 Fifth Ave., New York, New York 10016, United States
[#]School for Engineering of Matter, Transport and Energy, Arizona State University, Tempe, Arizona 85287, United States
[☆]National Institute for Materials Science, 1-1 Namiki, Tsukuba 305-0044, Japan
[▽]Department of Electrical, Computer & Systems Engineering, Rensselaer Polytechnic Institute, Troy, New York 12180, United States

Supporting Information

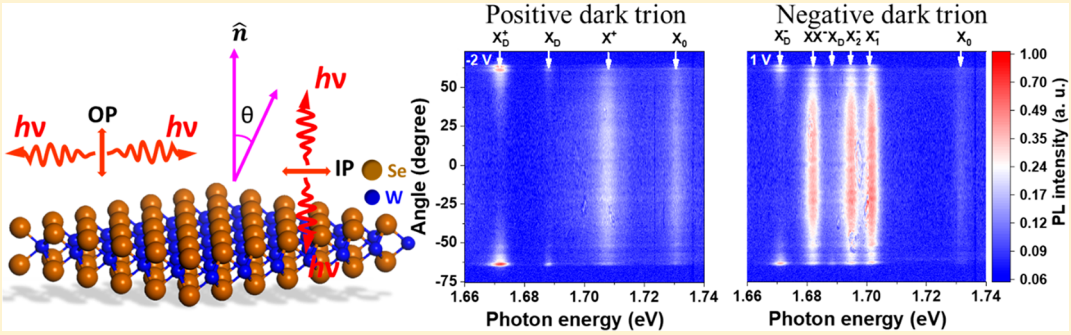

ABSTRACT: Spin-forbidden intravalley dark excitons in tungsten-based transition-metal dichalcogenides (TMDCs), because of their unique spin texture and long lifetime, have attracted intense research interest. Here, we show that we can control the dark exciton electrostatically by dressing it with one free electron or free hole, forming the dark trions. The existence of the dark trions is suggested by the unique magneto-photoluminescence spectroscopy pattern of the boron nitride (BN)-encapsulated monolayer WSe_2 device at low temperature. The unambiguous evidence of the dark trions is further obtained by directly resolving the radiation pattern of the dark trions through back focal plane imaging. The dark trions possess a binding energy of ∼15 meV, and they inherit the long lifetime and large *g*-factor from the dark exciton. Interestingly, under the out-of-plane magnetic field, dressing the dark exciton with one free electron or hole results in distinctively different valley polarization of the emitted photon, as a result of the different intervalley scattering mechanism for the electron and hole. Finally, the lifetime of the positive dark trion can be further tuned from ∼50 ps to ∼215 ps by controlling the gate voltage. The gate-tunable dark trions usher in new opportunities for excitonic optoelectronics and valleytronics.

KEYWORDS: *dark trion, magneto-PL, Fourier plane imaging, valley polarization, TRPL*

Because of the reduced screening and enhanced Coulomb interactions, monolayer transition-metal dichalcogenides (TMDCs) host excitons with large binding energy, on the order of hundreds of meV.[1−4] Because of the lack of inversion symmetry and the 3-fold rotation symmetry, the excitons in TMDCs possess the valley degree of freedom, which can be accessed through left or right circularly polarized light, which selectively excites the excitons at the K or K′ valley (corners of the Brillouin zone).[5−12] The large spin−orbit coupling-induced valence band splitting ensures the spin-valley locking,[2,13−15] which results in the robust valley-polarized photoluminescence (PL), even at room temperature.[16−19] However, the excitons are short-lived, with a typical lifetime in the range of a few to

Received: May 25, 2019
Revised: August 21, 2019
Published: September 5, 2019

DOI: 10.1021/acs.nanolett.9b02132
Nano Lett. 2019, 19, 6886−6893

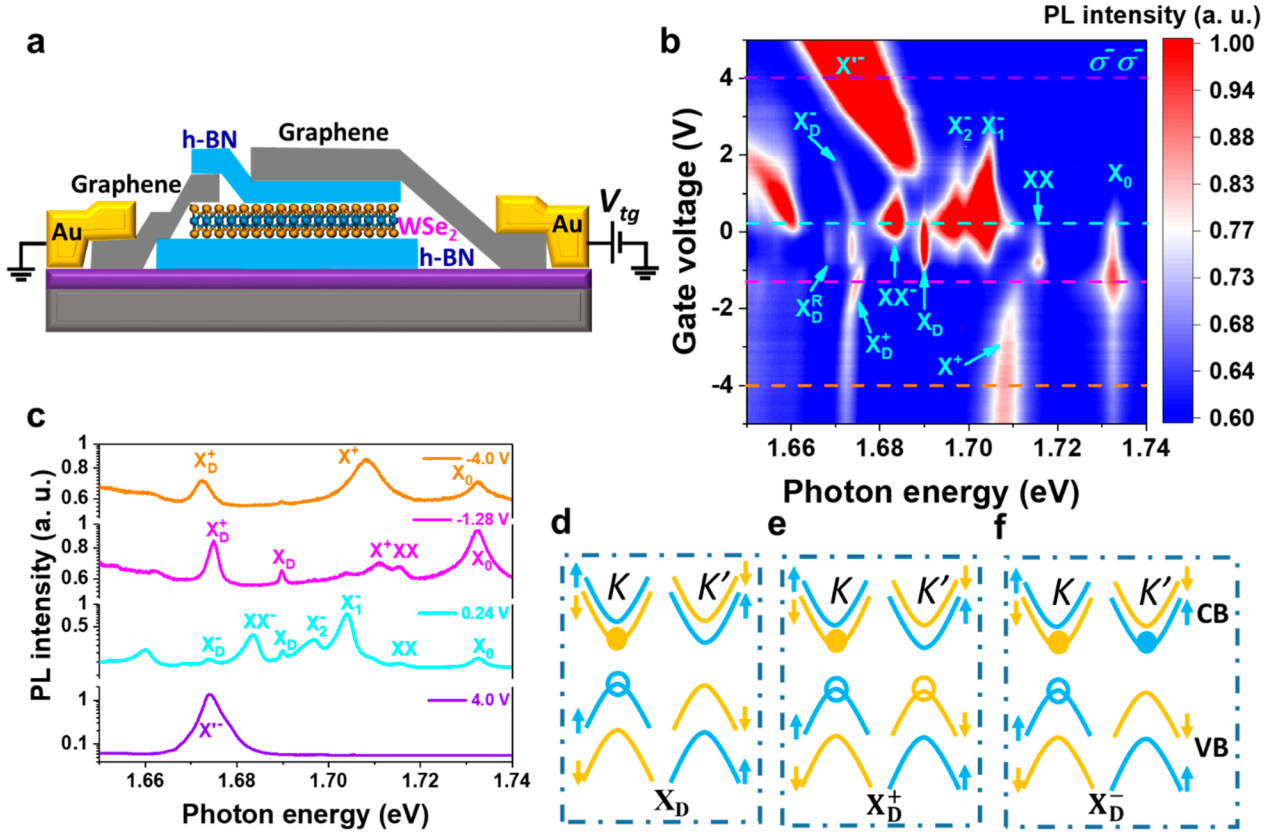

Figure 1. Gate-dependent PL spectroscopy of the BN encapsulated monolayer WSe_2 device. (a) Schematic representation of the BN encapsulated monolayer WSe_2 device. One piece of few-layer graphene is used as the electrode and another piece is used as the top gate electrode. (b) PL spectra at 4.2 K, as a function of the top gate voltage for the BN-encapsulated monolayer WSe_2 device. The color represents the PL intensity. The excitation is a CW laser centered at 1.879 eV with an excitation power of 40 μW. (c) PL spectra at the gate voltages of −4.0, −1.28, 0.24, and 4.0 V, respectively, corresponding to the dashed lines in panel (b). (d−f) Schemes of the dark exciton (X_D, panel (d)), positive dark trion (X_D^+, panel (e)), and negative dark trion (X_D^-, panel (f)).

tens of picoseconds,[20−22] which significantly limits potential applications.

Recently, it has been discovered that tungsten-based TMDCs such as WSe_2 and WS_2 have a unique bandstructure, in which the spin−orbit coupling also induces the splitting of the conduction band.[23−25] However, the resulting ground state of the exciton is a spin-triplet state that prevents direct recombination, hence referenced as the spin-forbidden dark exciton.[22,25−28] The existence of such a long-lived dark exciton has been revealed through the application of an in-plane magnetic field,[25] coupling to a plasmonic substrate,[28] directly observing PL from the side,[27] or collecting PL signals with an objective of large numerical aperture (NA).[29−32]

The spin-forbidden dark exciton, nonetheless, can also radiate through a finite out-of-plane dipole moment, which does not obey the same valley physics as the bright exciton, which arises from the combination of the inversion symmetry breaking and 3-fold rotation symmetry that restricts the in-plane dipole radiation.[28,33] As a result, we previously found that the valley-resolved PL spectra under an out-of-plane magnetic field exhibit a unique "cross" pattern in the intrinsic regime, distinctively different from other excitonic complexes.[29−31] Here, we apply magneto-PL spectroscopy to investigate a top-gated monolayer WSe_2 device and found a similar pattern in the *n*- or *p*-doped WSe_2. We attribute this pattern to the dark trions, which are dark excitons bound to free electrons or holes. Moreover, the existence of the dark trions is unambiguously demonstrated by directly resolving the radiation angle of the dark trions through back focal plane imaging. The binding energy of the dark trions, determined by the PL peak position difference between the dark trions and dark exciton, is found to be ∼15 meV. Interestingly, we found the asymmetric valley polarization behavior of the positive and negative trions in the presence of the out-of-plane magnetic field, originating from the different intervalley scattering mechanism of the electron and hole. The dark trions also inherit the large *g*-factor of the dark exciton (approximately −9), leading to a large Zeeman splitting of ∼9.0 meV under the magnetic field of 17 T. The direct observation and improved understanding of the dark trions pave the way of exploiting the charged dark exciton for optoelectronic and valleytronics applications.

The boron nitride (BN)-encapsulated monolayer WSe_2 device is fabricated through a pickup method as described in previous works,[29,34−36] and it is shown schematically in Figure 1a. The monolayer WSe_2 is contacted by a few-layer graphene electrode and is also gated through a few-layer graphene as the top gate electrode, with the top BN flake working as the gate dielectric. The high quality of monolayer WSe_2 is demonstrated through the well-resolved excitonic fine structures in the gate-dependent PL spectra at 4.2 K (see Figures 1b and 1c). Most of the excitonic complexes have been identified previously, including the bright exciton (X_0), the biexciton (XX) and charged biexciton (XX^-),[29−32,37−39] the positive

DOI: 10.1021/acs.nanolett.9b02132
Nano Lett. 2019, 19, 6886−6893

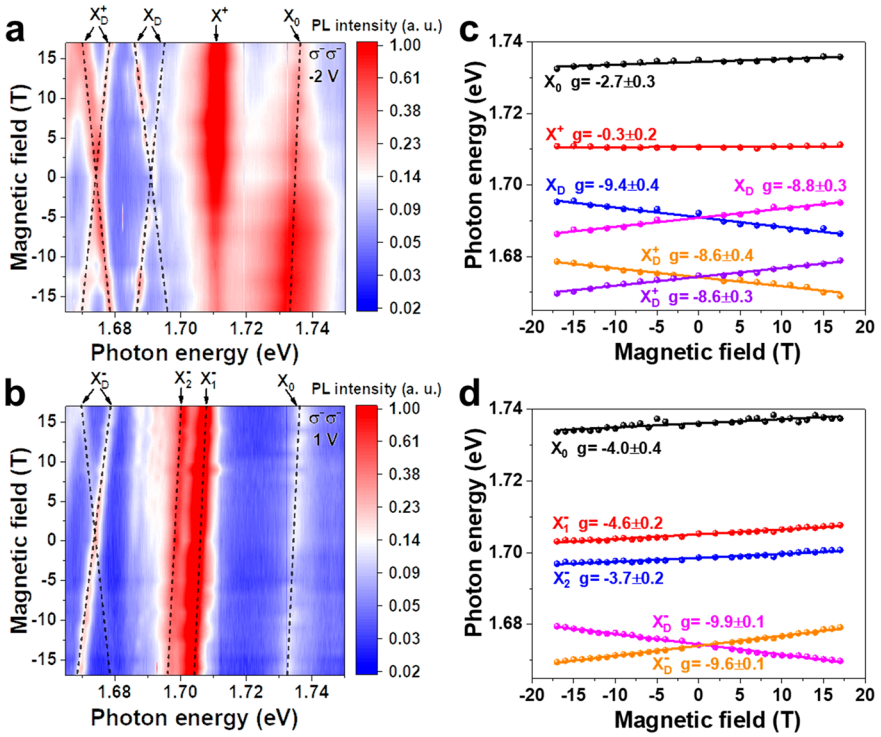

Figure 2. Gate-dependent magneto-PL spectroscopy of monolayer WSe_2: (a, b) Color plots of the PL spectra, as a function of the magnetic field for the gate voltage of −2 V (hole-doped) and 1 V (electron-doped), respectively; and (c, d) PL peak shift for different excitonic complexes extracted from panels (a) and (b). The Zeeman shift of each peak is utilized to calculate the associated *g*-factor through a linear fitting, for gate voltages of −2.0 and 1.0 V, respectively.

bright trion (X^+), the two negative trions (X_1^- and X_2^-),[8,23,40,41] and the dark exciton replica (X_D^R).[42] In particular, the PL peak centered at 1.690 eV, with the intensity maximized in the nearly charge neutral region (gate voltage between approximately −1.0 V to ∼0.35 V), has been identified as the spin-forbidden dark exciton (X_D) previously.[22,25−28,33] The spin-forbidden X_D, schematically shown in Figure 1d, arises from the unique band structure of WSe_2, in which the spin−orbit coupling-induced conduction band splitting leads to a conduction band minimum (CBM) with spin opposite to that of the valence band maximum (VBM). As a result, the ground state of the optical excitation-generated exciton is a spin-triplet state and its direct recombination is spin-forbidden.

The valley-resolved magneto-PL spectra have been previously employed to identify the dark exciton in charge-neutral WSe_2. When the WSe_2 is excited with a circularly polarized light (for example, σ^-), the radiation from the out-of-plane dipole is p-polarized and will give rise to both left (σ^-) and right (σ^+) circularly polarized PL emission in our detection scheme, which have different energies under the out-of-plane magnetic field, a result of the opposite Zeeman splitting for the exciton in K and K′ valleys.[16−19,37,43−46] Therefore, for charge-neutral WSe_2, the valley resolved magneto-PL spectra in the $\sigma^-\sigma^-$ configuration (see the Supporting Information (SI)), which represents the left-circular polarized excitation and left-circular polarized detection, show that the PL peak corresponding to X_D splits into two branches, while the other excitonic complexes, such as X_0, exhibit a linear Zeeman shift. In this study, we found that as we gate the WSe_2 to the hole-doping (gate voltage of −2.0 V) and electron-doping regime (gate voltage of 1.0 V), the PL peaks centered at ∼1.675 and 1.674 eV with no magnetic field applied, labeled as X_D^+ and X_D^- in Figure 1b, exhibit similar "cross" patterns in the valley-resolved magneto-PL spectra shown in Figures 2a and 2b, respectively. We have also reproduced this observation in two other BN encapsulated WSe_2 devices (see the Supplementary Note 1 in the SI).

The positive dark trion and negative dark trion, schematically shown in Figures 1e and 1f, emit photons through the recombination of the electron and hole either in the K or K′ valley, same as the dark exciton (Figure 1d). As a result, in a noninteracting picture in which the Zeeman splitting is calculated through the individual shift of CBM and VBM associated with the recombination electron−hole pair,[29,47] the magneto-PL spectra of X_D^+ and X_D^- will share the same Zeeman splitting as the charge-neutral X_D. Therefore, we assign the emerging "cross" patterns in the hole-doped and electron-doped WSe_2 (see Figures 2a and 2b) to the positive dark trion and the negative dark trion, a neutral dark exciton bound to a free hole and an electron, respectively. We notice that a very recent report also utilizes the similar pattern in the magneto-PL spectra to identify the dark trions.[48]

This determination is also supported by the quantitative analysis of the Zeeman splitting.[16−19,28,35−38] The valley-Zeeman splitting can be expressed as $E^{K(K')} = E_0 \pm g\mu_B B$, where E_0 is the PL peak position at the absence of the external magnetic field, "+" or "−" corresponds to the shift in the K or K′ valley, g is the Landé *g*-factor, μ_B is the Bohr magneton, and B is the out-of-plane magnetic field. The Landé *g*-factor, as previously mentioned, can be calculated by counting the difference of the shift of the conducting band minimum (CBM) and valence band maximum (VBM) that are associated with the electron and hole involved in the recombination. The *g*-factor for X_D in this device is

DOI: 10.1021/acs.nanolett.9b02132
Nano Lett. 2019, 19, 6886−6893

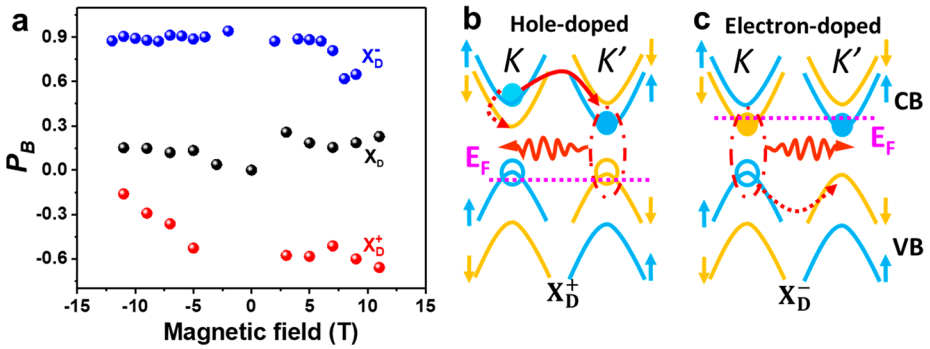

Figure 3. Valley polarization under the magnetic field. (a) Valley polarization (P_B) of negative dark trion, dark exciton, and positive dark trion under a magnetic field, $P_B = \frac{I(K') - I(K)}{I(K') + I(K)}\sigma(B)$, where $I(K)$ and $I(K')$ are the PL intensity from the K and K' valleys, respectively. $\sigma(B)$ is 1 or −1 for the positive or negative B field, respectively. (b, c) Schematics of electron and hole recombination for the positive dark trion (panel (b)) and negative dark trion (panel (c)), respectively.

approximately −9.5 (see the SI), which is consistent with the theoretical expectation of −8 and the previous experimentally reported value.[22,29,31] Figures 2c and 2d show that the g-factors of X_D^+ and X_D^- are approximately −8.6 and −9.8, respectively, similar to that of X_D, considering the fitting uncertainty, experimental uncertainty, and possible change of the g-factors with the increased doping level. According to our discussion, these agreements support the assignments of the positive dark trion and the negative dark trion, as the recombination electron−hole (e-h) pairs involved in the dark trion is the same as the charge-neutral dark exciton. The g-factor calculation is also confirmed from the data from other two devices (see Supplementary Notes 2 and 3 in the SI for the data from the second and third devices). The g-factors of X_D^+ and X_D^-, similar to that of X_D, are more than two times larger than that of X_0 (approximately −4.3).[19,29,49,50] As a result, the Zeeman splitting of the dark trions can be as large as ∼9.0 meV at the presence of an out-of-plane magnetic field of 17 T. The significant Zeeman splitting due to the large g-factor can be utilized for breaking the valley degeneracy.

Despite the similar binding energy, the negative and positive dark trions exhibit asymmetric behavior. The intensity of the negative dark trion is weaker than that of the positive dark trion (see Figures 1b and 1c), consistent with previous reports.[28,51] It is likely due to the existence of the lower energy states in the n-doped WSe_2, such as the one suggested by the bright PL peak near energy 1.660 eV in the n-doped WSe_2 (Figure 1b). Also note that, because of the weak PL intensity of the negative dark trion, the "cross" pattern is more difficult to observe in the n-doped WSe_2 (see Supplementary Notes 2 and 3). More interestingly, the split K and K' PL branches in the magneto-PL spectra are not of equal intensity for dark trions, in contrast to the case of the dark exciton[29,42] that has equal emission probability from the K and K' branches under the external out-of-plane magnetic field. In addition, the brighter branch of the negative dark trion (X_D^-) (with the intensity ratio ∼20 for the PL intensity between the two branches) is the same as the visible branch in the magneto-PL for the bright exciton (X_0), but the opposite to the brighter branch of the positive dark trion (X_D^+) (with an intensity ratio of ∼4). This means that dressing the dark exciton with one free hole or electron makes the dark trion to emit light more likely from one valley or the other, granting the valley information to the dark trion.

This information can be quantitatively shown in Figure 3. Since only one branch of the bright exciton is visible in the helicity-resolved PL spectra under the out-of-plane magnetic field, we define the valley polarization of the bright exciton under the magnetic field as $P_B = 1$. P_B is defined as $P_B = \frac{I(K') - I(K)}{I(K') + I(K)}\sigma(B)$, where $I(K')$ and $I(K)$ are the PL intensities for the K' valley and the K valley. $\sigma(B)$ is 1 or −1 for positive or negative B-field, respectively. It is evident from Figure 3a that the positive dark trion has a negative P_B value and the negative dark trion has a positive P_B value, while the dark exciton has P_B value close to zero as the PL intensity from the two branches are similar. The valley information granted by the additional electron or hole can be understood by the different intervalley scattering mechanism. For doped samples under weak optical excitation, the electron−hole recombination, which generates the emitted photon, is determined by the optically excited minority carrier (hole for the n-doped sample and electron for the p-doped sample). For the case of the electron-doped sample, optically excited hole determines the electron−hole recombination. It has been shown[52] that the intervalley scattering is less likely and the hole prefers to stay in the same valley as it is excited, for example, K valley (Figure 3c), and a photon will be emitted as a result of the e-h recombination in the K valley. As a result, the PL from the negative dark trion will exhibit the same valley polarization of the PL from the bright exciton. In the case of the p-doped sample, the e-h recombination will be determined by the optically excited electron. However, the intervalley scattering of electrons is much faster. In particular, the electron in the second conduction band (shown in Figure 3b) could be more likely to scatter to the other valley, because of efficient coupling to the K-point phonons, compared with the possibility of relaxing to the first CBM in the same valley, since it requires flipping the spin. As a result, the emitted photon will arise from the e-h recombination in the other valley (K' in Figure 3b), which has the opposite valley polarization as the bright exciton. In the presence of the out-of-plane magnetic field, the energy degeneracy between the K valley and the K' valley is lifted, and the valley information on the emitted photon can be resolved in the magneto-PL spectra as the two well-resolved branches (see Figures 2a and 2b). The higher valley polarization of the negative dark trion, stemming from the prohibitive intervalley scattering of the hole, makes it an ideal candidate for valleytronics applications.

DOI: 10.1021/acs.nanolett.9b02132
Nano Lett. 2019, 19, 6886−6893

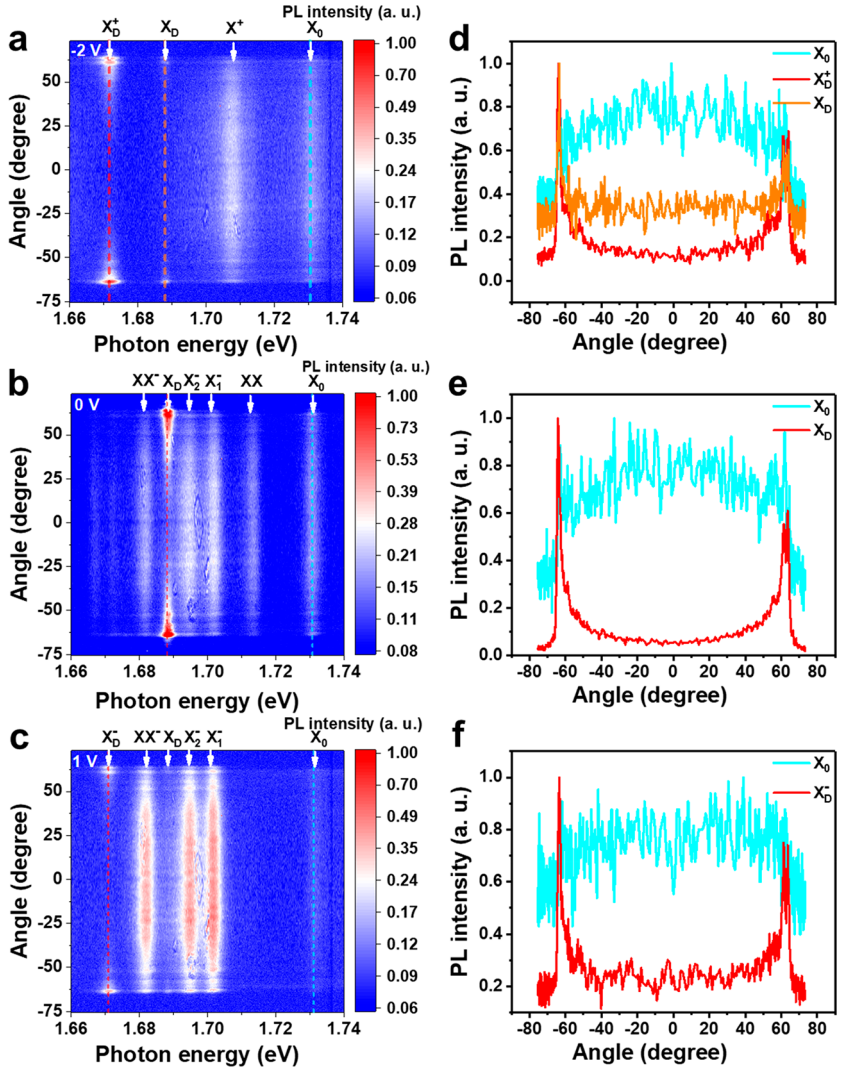

Figure 4. Back focal plane imaging of the PL radiation pattern for different excitonic complexes. (a–c) Color plots of PL intensity for different excitonic complexes, as a function of the emitted photon energy and the radiation angle. The radiation angle is resolved through imaging the back focal plane directly. Plots show experimental data obtained for top gate voltages of −2 V (panel (a)), 0 V (panel (b)), and 1 V (panel (c)), revealing the radiation pattern for the positive dark trion, dark exciton, and negative dark trion, respectively. (d–f) PL intensity as a function of the radiation angle (vertical line cut in panels (a)–(c)) of the positive dark trion, dark exciton, and negative dark trion in the corresponding color plot, compared with the bright exciton (X_0) PL intensity at the same gate voltage.

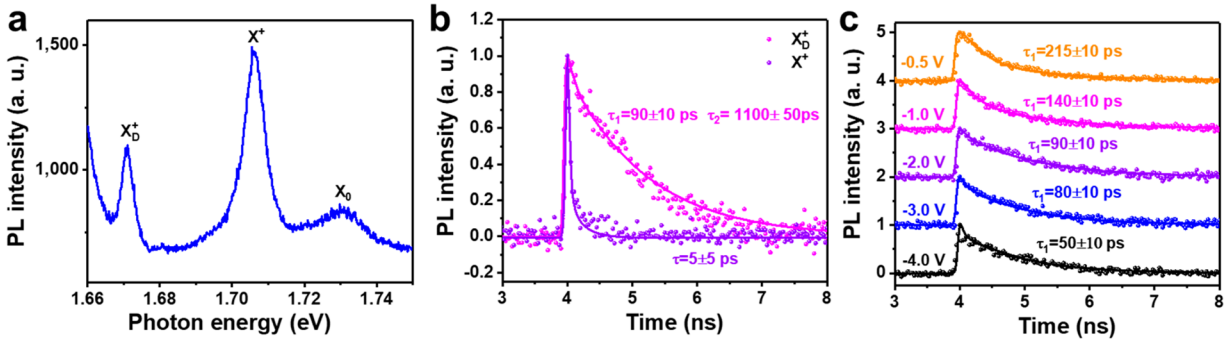

Figure 5. Time-resolved PL spectra of X_D^+ of monolayer WSe_2. (a) PL spectrum with a pulse laser excitation centered at 1.908 eV at 42 K, with the excitation power of 50 μW and the gate voltage of −2.5 V. (b) Comparison of the TRPL spectra of the positive bright trion (p-trion, purple) and positive dark trion (magenta) at the gate voltage of −2.0 V. The time-resolved PL data (dotted lines) are convoluted (solid lines) with IRF, using a single exponential function $I = A\exp(-t/\tau)$ for X^+ and a biexponential function $I = A_1\exp(-t_1/\tau_1) + A_2\exp(-t_2/\tau_2)$ for X_D^+. (c) TRPL spectra of the positive dark trion as a function of the gate voltage (dots), with the extracted lifetime for the fast component shown.

DOI: 10.1021/acs.nanolett.9b02132
Nano Lett. 2019, 19, 6886–6893

Considering the complexity of valley polarization associated with the dressing of free carriers and especially the weak PL from the negative dark trion, the "cross" pattern could be hard to resolve, especially for the negative dark trion with relatively weak PL (see Supplementary Notes 2 and 3). Therefore, direct evidence of the dark trion is needed. Since the dark trions also radiate through the out-of-plane dipole as the dark exciton, the radiation pattern of the dark trion, if can be resolved, will be the unambiguous evidence of the dark trion. We achieved this by directly imaging the back focal plane,[53] which is a Fourier transform of the real space image and has been used to resolve the energy dispersion in momentum space for photonic cavity.[54,55] Recently it has been applied to resolve the exciton radiation pattern of the 2D semiconductor.[30,56] Here, we resolve the spectra information on the PL using the horizontal array of the pixels of the silicon charge-coupled device (CCD) and resolve the radiation angle, defined here as the angle from the normal, using the vertical array of the CCD camera (schematic setup shown in Supplementary Note 4 in the SI).

The spectral-resolved and radiation-angle-resolved experimental data at 4.2 K are shown in Figure 4. It is evident that the radiation pattern of the dark trion (Figure 4a and 4c) is distinctively different from other excitonic complexes, such as the bright exciton, but the same as that of the dark exciton (Figure 4b). The maximum PL intensity observed for the dark trions or the dark exciton is located at ∼64°, limited by the NA (∼0.9) of our objective. In contrast, the PL intensity of the bright exciton is maximized at ∼0°. The direct observation of the radiation pattern thus provides a decisive determination of the dark trions.

Finally, the well-resolved different excitonic peaks allow us to reveal the dynamics of the positive dark trion through time-resolved PL (TRPL) measurement directly.[42] Figure 5a shows the PL spectrum obtained with a pulse laser excitation at 1.908 eV at 42 K, with an excitation power of 50 μW and a gate voltage of −2.5 V, and X_D^+ and X^+ are well-resolved. Since both X_D^+ and X^+ are charge-neutral excitons bound to a free hole, we assume the dielectric environment is similar at the same gate voltage, and we can directly compare the lifetimes of these two types of *p*-trions. The TRPL spectra (dots) for X_D^+ and X^+ are presented in Figure 5b, and the lifetimes are extracted by the convolution of the instrument response function (IRF) (solid lines) with a single exponential function $I = Ae^{-t/\tau}$ for X^+ and a biexponential function $I = A_1 \exp(-t_1/\tau_1) + A_2 \exp(-t_2/\tau_2)$ for X_D^+, respectively.[57−60] The results indicate that the lifetime of X^+ only shows a fast component while that of X_D^+ exhibits both a dominant fast component and a slow component (see Supplementary Note 4 for a detailed analysis). We attribute the slow component to the contribution from the residue of the possible slowly decaying PL from defects and thus use the fast component as the dark trion lifetime to compare with that of X^+. As shown in Figure 5b, at the gate voltage of −2 V, the lifetime of X_D^+ (∼90 ps) is more than 10 times longer than that of X^+ (∼5 ps), which confirms that the positive dark trion inherits the long lifetime from the dark exciton.[20,22,25,37] The lifetime of the dark trion is also a sensitive function of the gate voltage. As shown in Figure 5c, the lifetime of X_D^+ can be tuned from ∼215 ps to ∼50 ps as we change the gate voltage from −0.5 V to −4 V, which is expected as the increased hole doping increases the nonradiative channels and decreases the positive dark trion lifetime. The long lifetime of ∼215 ps in the slight *n*-doped WSe_2 is comparable to that of the charge-neutral dark exciton (∼250 ps) reported previously.[42]

In summary, we have directly observed the dark trions through the back focal plane imaging of the radiation pattern of BN-encapsulated monolayer WSe_2. The binding energy is determined to be ∼15 meV. The large *g*-factor (approximately −9) of the dark trions can be utilized to break valley degeneracy through an external magnetic field or proximity field effects.[61,62] The discovery of the dark trions illustrates a new way to tune the dark exciton complexes in WSe_2 through electrostatic gating. Dressing the dark exciton with the additional free carrier encodes the valley information into the otherwise valley-depolarized dark exciton. In addition, the lifetime of the dark trion can be sensitively changed from ∼215 ps to ∼50 ps by controlling the doping. The dark trions therefore open the door to new possibilities of valleytronics and excitonic applications.

■ ASSOCIATED CONTENT

Supporting Information

The Supporting Information is available free of charge on the ACS Publications website at DOI: 10.1021/acs.nanolett.9b02132.

Additional information on the gate-voltage and magnetic field dependent PL, radiation pattern detection technique, and the detail of extracted lifetime from convolution (PDF)

■ AUTHOR INFORMATION

Corresponding Author

*E-mail: shis2@rpi.edu.

ORCID

Sefaattin Tongay: 0000-0001-8294-984X
Vinod M. Menon: 0000-0002-9725-6445
Dmitry Smirnov: 0000-0001-6358-3221
Su-Fei Shi: 0000-0001-5158-805X

Author Contributions

¶These authors contributed equally to this work.

Notes

The authors declare no competing financial interest.

■ ACKNOWLEDGMENTS

We thank Dr. Lei Shi and Shengnan Miao for helpful discussions. Z. Li and S.-F.S. acknowledge support from the Air Force Office of Scientific Research (AFOSR), through Grant No. FA9550-18-1-0312. T.W. and S.-F.S. acknowledge support from ACS PRF, through Grant No. 59957-DNI10. Z.L. and S.-F.S. acknowledge support from NYSTAR, through Focus Center-NY-RPI Contract No. C150117. S.T. acknowledges support from the National Science Foundation (NSF) (Nos. DMR-1552220 and DMR 1838443). The device fabrication was supported by Micro and Nanofabrication Clean Room (MNCR) at Rensselaer Polytechnic Institute (RPI). K.W. and T.T. acknowledge support from the Elemental Strategy Initiative conducted by the MEXT, Japan and the CREST (JPMJCR15F3), JST. Z. Lu and D.S. acknowledge support from the U.S. Department of Energy (No. DE-FG02-07ER46451) for magneto-photoluminescence measurements performed at the National High Magnetic Field Laboratory, which is supported by National Science Foundation through NSF/DMR-1644779 and the State of Florida. S.-F.S. also acknowledges the support from a KIP grant from RPI.

DOI: 10.1021/acs.nanolett.9b02132
Nano Lett. 2019, 19, 6886−6893

REFERENCES

(1) Ugeda, M. M.; Bradley, A. J.; Shi, S.-F.; da Jornada, F. H.; Zhang, Y.; Qiu, D. Y.; Ruan, W.; Mo, S.-K.; Hussain, Z.; Shen, Z.-X.; Wang, F.; Louie, S. G.; Crommie, M. F. Giant Bandgap Renormalization and Excitonic Effects in a Monolayer Transition Metal Dichalcogenide Semiconductor. *Nat. Mater.* **2014**, *13*, 1091−1095.

(2) Chernikov, A.; Berkelbach, T. C.; Hill, H. M.; Rigosi, A.; Li, Y.; Aslan, O. B.; Reichman, D. R.; Hybertsen, M. S.; Heinz, T. F. Exciton Binding Energy and Nonhydrogenic Rydberg Series in Monolayer WS_2. *Phys. Rev. Lett.* **2014**, *113*, 076802.

(3) Ye, Z.; Cao, T.; O'Brien, K.; Zhu, H.; Yin, X.; Wang, Y.; Louie, S. G.; Zhang, X. Probing Excitonic Dark States in Single-Layer Tungsten Disulphide. *Nature* **2014**, *513*, 214−218.

(4) He, K.; Kumar, N.; Zhao, L.; Wang, Z.; Mak, K. F.; Zhao, H.; Shan, J. Tightly Bound Excitons in Monolayer WSe_2. *Phys. Rev. Lett.* **2014**, *113*, 026803.

(5) Xiao, D.; Liu, G.-B.; Feng, W.; Xu, X.; Yao, W. Coupled Spin and Valley Physics in Monolayers of MoS_2 and Other Group-VI Dichalcogenides. *Phys. Rev. Lett.* **2012**, *108*, 196802.

(6) Gong, Z.; Liu, G.-B.; Yu, H.; Xiao, D.; Cui, X.; Xu, X.; Yao, W. Magnetoelectric Effects and Valley-Controlled Spin Quantum Gates in Transition Metal Dichalcogenide Bilayers. *Nat. Commun.* **2013**, *4*, 2053.

(7) Ye, Z.; Sun, D.; Heinz, T. F. Optical Manipulation of Valley Pseudospin. *Nat. Phys.* **2017**, *13*, 26−29.

(8) Plechinger, G.; Nagler, P.; Arora, A.; Schmidt, R.; Chernikov, A.; Del Águila, A. G.; Christianen, P. C. M.; Bratschitsch, R.; Schüller, C.; Korn, T. Trion Fine Structure and Coupled Spin-Valley Dynamics in Monolayer Tungsten Disulfide. *Nat. Commun.* **2016**, *7*, 12715.

(9) Mak, K. F.; Shan, J. Photonics and Optoelectronics of 2D Semiconductor Transition Metal Dichalcogenides. *Nat. Photonics* **2016**, *10*, 216−226.

(10) Xu, X.; Yao, W.; Xiao, D.; Heinz, T. F. Spin and Pseudospins in Layered Transition Metal Dichalcogenides. *Nat. Phys.* **2014**, *10*, 343−350.

(11) Cao, T.; Wang, G.; Han, W.; Ye, H.; Zhu, C.; Shi, J.; Niu, Q.; Tan, P.; Wang, E.; Liu, B.; Feng, J. Valley-Selective Circular Dichroism of Monolayer Molybdenum Disulphide. *Nat. Commun.* **2012**, *3*, 885−887.

(12) Mak, K. F.; He, K.; Shan, J.; Heinz, T. F. Control of Valley Polarization in Monolayer MoS_2 by Optical Helicity. *Nat. Nanotechnol.* **2012**, *7*, 494−498.

(13) Liu, G.-B.; Shan, W. Y.; Yao, Y.; Yao, W.; Xiao, D. Three-Band Tight-Binding Model for Monolayers of Group-VIB Transition Metal Dichalcogenides. *Phys. Rev. B: Condens. Matter Mater. Phys.* **2013**, *88*, 085433.

(14) Schaibley, J. R.; Yu, H.; Clark, G.; Rivera, P.; Ross, J. S.; Seyler, K. L.; Yao, W.; Xu, X. Valleytronics in 2D Materials. *Nat. Rev. Mater.* **2016**, *1*, 16055.

(15) Schneider, C.; Glazov, M. M.; Korn, T.; Höfling, S.; Urbaszek, B. Two-Dimensional Semiconductors in the Regime of Strong Light-Matter Coupling. *Nat. Commun.* **2018**, *9*, 2695.

(16) Li, Y.; Ludwig, J.; Low, T.; Chernikov, A.; Cui, X.; Arefe, G.; Kim, Y. D.; Van Der Zande, A. M.; Rigosi, A.; Hill, H. M.; Kim, S. H.; Hone, J.; Li, Z.; Smirnov, D.; Heinz, T. F. Valley Splitting and Polarization by the Zeeman Effect in Monolayer $MoSe_2$. *Phys. Rev. Lett.* **2014**, *113*, 266804.

(17) Macneill, D.; Heikes, C.; Mak, K. F.; Anderson, Z.; Kormányos, A.; Zólyomi, V.; Park, J.; Ralph, D. C. Breaking of Valley Degeneracy by Magnetic Field in Monolayer $MoSe_2$. *Phys. Rev. Lett.* **2015**, *114*, 037401.

(18) Aivazian, G.; Gong, Z.; Jones, A. M.; Chu, R.-L.; Yan, J.; Mandrus, D. G.; Zhang, C.; Cobden, D.; Yao, W.; Xu, X. Magnetic Control of Valley Pseudospin in Monolayer WSe_2. *Nat. Phys.* **2015**, *11*, 148−152.

(19) Srivastava, A.; Sidler, M.; Allain, A. V.; Lembke, D. S.; Kis, A.; Imamoglu, A. Valley Zeeman Effect in Elementary Optical Excitations of Monolayer WSe_2. *Nat. Phys.* **2015**, *11*, 141−147.

(20) Robert, C.; Lagarde, D.; Cadiz, F.; Wang, G.; Lassagne, B.; Amand, T.; Balocchi, A.; Renucci, P.; Tongay, S.; Urbaszek, B.; Marie, X. Exciton Radiative Lifetime in Transition Metal Dichalcogenide Monolayers. *Phys. Rev. B: Condens. Matter Mater. Phys.* **2016**, *93*, 205423.

(21) Lagarde, D.; Bouet, L.; Marie, X.; Zhu, C. R.; Liu, B. L.; Amand, T.; Tan, P. H.; Urbaszek, B. Carrier and Polarization Dynamics in Monolayer MoS_2. *Phys. Rev. Lett.* **2014**, *112*, 047401.

(22) Robert, C.; Amand, T.; Cadiz, F.; Lagarde, D.; Courtade, E.; Manca, M.; Taniguchi, T.; Watanabe, K.; Urbaszek, B.; Marie, X. Fine Structure and Lifetime of Dark Excitons in Transition Metal Dichalcogenide Monolayers. *Phys. Rev. B: Condens. Matter Mater. Phys.* **2017**, *96*, 155423.

(23) Yu, H.; Liu, G.-B.; Gong, P.; Xu, X.; Yao, W. Dirac Cones and Dirac Saddle Points of Bright Excitons in Monolayer Transition Metal Dichalcogenides. *Nat. Commun.* **2014**, *5*, 3876.

(24) Mak, K. F.; Lee, C.; Hone, J.; Shan, J.; Heinz, T. F. Atomically Thin MoS_2: A New Direct-Gap Semiconductor. *Phys. Rev. Lett.* **2010**, *105*, 136805.

(25) Zhang, X. X.; Cao, T.; Lu, Z.; Lin, Y. C.; Zhang, F.; Wang, Y.; Li, Z.; Hone, J. C.; Robinson, J. A.; Smirnov, D.; Louie, S. G.; Heinz, T. F. Magnetic Brightening and Control of Dark Excitons in Monolayer WSe_2. *Nat. Nanotechnol.* **2017**, *12*, 883−888.

(26) Zhang, X. X.; You, Y.; Zhao, S. Y. F.; Heinz, T. F. Experimental Evidence for Dark Excitons in Monolayer WSe_2. *Phys. Rev. Lett.* **2015**, *115*, 257403.

(27) Wang, G.; Robert, C.; Glazov, M. M.; Cadiz, F.; Courtade, E.; Amand, T.; Lagarde, D.; Taniguchi, T.; Watanabe, K.; Urbaszek, B.; Marie, X. In-Plane Propagation of Light in Transition Metal Dichalcogenide Monolayers: Optical Selection Rules. *Phys. Rev. Lett.* **2017**, *119*, 047401.

(28) Zhou, Y.; Scuri, G.; Wild, D. S.; High, A. A.; Dibos, A.; Jauregui, L. A.; Shu, C.; De Greve, K.; Pistunova, K.; Joe, A. Y.; Taniguchi, T.; Watanabe, K.; Kim, P.; Lukin, M. D.; Park, H. Probing Dark Excitons in Atomically Thin Semiconductors via Near-Field Coupling to Surface Plasmon Polaritons. *Nat. Nanotechnol.* **2017**, *12*, 856−860.

(29) Li, Z.; Wang, T.; Lu, Z.; Jin, C.; Chen, Y.; Meng, Y.; Lian, Z.; Taniguchi, T.; Watanabe, K.; Zhang, S.; Smirnov, D.; Shi, S.-F. Revealing the Biexciton and Trion-Exciton Complexes in BN Encapsulated WSe_2. *Nat. Commun.* **2018**, *9*, 3719.

(30) Ye, Z.; Waldecker, L.; Ma, E. Y.; Rhodes, D.; Antony, A.; Kim, B.; Zhang, X. X.; Deng, M.; Jiang, Y.; Lu, Z.; Smirnov, D.; Watanabe, K.; Taniguchi, T.; Hone, J.; Heinz, T. F. Efficient Generation of Neutral and Charged Biexcitons in Encapsulated WSe_2 Monolayers. *Nat. Commun.* **2018**, *9*, 3718.

(31) Chen, S.-Y.; Goldstein, T.; Taniguchi, T.; Watanabe, K.; Yan, J. Coulomb-Bound Four- and Five-Particle Intervalley States in an Atomically-Thin Semiconductor. *Nat. Commun.* **2018**, *9*, 3717.

(32) Barbone, M.; Montblanch, A. R.-P.; Kara, D. M.; Palacios-Berraquero, C.; Cadore, A. R.; De Fazio, D.; Pingault, B.; Mostaani, E.; Li, H.; Chen, B.; Watanabe, K.; Taniguchi, T.; Tongay, S.; Wang, G.; Ferrari, A. C.; Atatüre, M. Charge-Tuneable Biexciton Complexes in Monolayer WSe_2. *Nat. Commun.* **2018**, *9*, 3721.

(33) Park, K. D.; Jiang, T.; Clark, G.; Xu, X.; Raschke, M. B. Radiative Control of Dark Excitons at Room Temperature by Nano-Optical Antenna-Tip Purcell Effect. *Nat. Nanotechnol.* **2018**, *13*, 59−64.

(34) Pizzocchero, F.; Gammelgaard, L.; Jessen, B. S.; Caridad, J. M.; Wang, L.; Hone, J.; Bøggild, P.; Booth, T. J. The Hot Pick-up Technique for Batch Assembly of van Der Waals Heterostructures. *Nat. Commun.* **2016**, *7*, 11894.

(35) Cao, Y.; Luo, J. Y.; Fatemi, V.; Fang, S.; Sanchez-Yamagishi, J. D.; Watanabe, K.; Taniguchi, T.; Kaxiras, E.; Jarillo-Herrero, P. Superlattice-Induced Insulating States and Valley-Protected Orbits in Twisted Bilayer Graphene. *Phys. Rev. Lett.* **2016**, *117*, 116804.

(36) Wang, L.; Meric, I.; Huang, P. Y.; Gao, Q.; Gao, Y.; Tran, H.; Taniguchi, T.; Watanabe, K.; Campos, L. M.; Muller, D. A.; Guo, J.; Kim, P.; Hone, J.; Shepard, K. L.; Dean, C. R. One-Dimensional

DOI: 10.1021/acs.nanolett.9b02132
Nano Lett. 2019, 19, 6886−6893

Electrical Contact to a Two-Dimensional Material. *Science* **2013**, *342*, 614−617.
(37) Nagler, P.; Ballottin, M. V.; Mitioglu, A. A.; Durnev, M. V.; Taniguchi, T.; Watanabe, K.; Chernikov, A.; Schüller, C.; Glazov, M. M.; Christianen, P. C. M.; Korn, T. Zeeman Splitting and Inverted Polarization of Biexciton Emission in Monolayer WS_2. *Phys. Rev. Lett.* **2018**, *121*, 57402.
(38) You, Y.; Zhang, X. X.; Berkelbach, T. C.; Hybertsen, M. S.; Reichman, D. R.; Heinz, T. F. Observation of Biexcitons in Monolayer WSe_2. *Nat. Phys.* **2015**, *11*, 477−481.
(39) Hao, K.; Specht, J. F.; Nagler, P.; Xu, L.; Tran, K.; Singh, A.; Dass, C. K.; Schuller, C.; Korn, T.; Richter, M.; Knorr, A.; Li, X.; Moody, G. Neutral and Charged Inter-Valley Biexcitons in Monolayer $MoSe_2$. *Nat. Commun.* **2017**, *8*, 15552.
(40) Jones, A. M.; Yu, H.; Schaibley, J. R.; Yan, J.; Mandrus, D. G.; Taniguchi, T.; Watanabe, K.; Dery, H.; Yao, W.; Xu, X. Excitonic Luminescence Upconversion in a Two-Dimensional Semiconductor. *Nat. Phys.* **2016**, *12*, 323−327.
(41) Singh, A.; Tran, K.; Kolarczik, M.; Seifert, J.; Wang, Y.; Hao, K.; Pleskot, D.; Gabor, N. M.; Helmrich, S.; Owschimikow, N.; Woggon, U.; Li, X. Long-Lived Valley Polarization of Intravalley Trions in Monolayer WSe_2. *Phys. Rev. Lett.* **2016**, *117*, 257402.
(42) Li, Z.; Wang, T.; Jin, C.; Lu, Z.; Lian, Z.; Meng, Y.; Blei, M.; Gao, S.; Taniguchi, T.; Watanabe, K.; Ren, T.; Tongay, S.; Yang, L.; Smirnov, D.; Cao, T.; Shi, S. F. Emerging Photoluminescence from the Dark-Exciton Phonon Replica in Monolayer WSe_2. *Nat. Commun.* **2019**, *10*, 2469.
(43) Stier, A. V.; McCreary, K. M.; Jonker, B. T.; Kono, J.; Crooker, S. A. Exciton Diamagnetic Shifts and Valley Zeeman Effects in Monolayer WS_2 and MoS_2 to 65 T. *Nat. Commun.* **2016**, *7*, 10643.
(44) Jiang, C.; Liu, F.; Cuadra, J.; Huang, Z.; Li, K.; Rasmita, A.; Srivastava, A.; Liu, Z.; Gao, W. B. Zeeman Splitting via Spin-Valley-Layer Coupling in Bilayer $MoTe_2$. *Nat. Commun.* **2017**, *8*, 802.
(45) Nagler, P.; Ballottin, M. V.; Mitioglu, A. A.; Mooshammer, F.; Paradiso, N.; Strunk, C.; Huber, R.; Chernikov, A.; Christianen, P. C. M.; Schüller, C.; Korn, T. Giant Zeeman Splitting Inducing Near-Unity Valley Polarization in van Der Waals Heterostructures. *Nat. Commun.* **2017**, *8*, 1551.
(46) Arora, A.; Schmidt, R.; Schneider, R.; Molas, M. R.; Breslavetz, I.; Potemski, M.; Bratschitsch, R. Valley Zeeman Splitting and Valley Polarization of Neutral and Charged Excitons in Monolayer $MoTe_2$ at High Magnetic Fields. *Nano Lett.* **2016**, *16*, 3624−3629.
(47) Rybkovskiy, D. V.; Gerber, I. C.; Durnev, M. V. Atomically Inspired k · p Approach and Valley Zeeman Effect in Transition Metal Dichalcogenide Monolayers. *Phys. Rev. B: Condens. Matter Mater. Phys.* **2017**, *95*, 155406.
(48) Liu, E.; van Baren, J.; Lu, Z.; Altaiary, M. M.; Taniguchi, T.; Watanabe, K.; Smirnov, D.; Lui, C. H. Gate Tunable Dark Trions in Monolayer WSe_2. *Phys. Rev. Lett.* **2019**, *123*, 027401.
(49) Mitioglu, A. A.; Plochocka, P.; Granados Del Aguila, Á.; Christianen, P. C. M.; Deligeorgis, G.; Anghel, S.; Kulyuk, L.; Maude, D. K. Optical Investigation of Monolayer and Bulk Tungsten Diselenide (WSe_2) in High Magnetic Fields. *Nano Lett.* **2015**, *15*, 4387−4392.
(50) Wang, G.; Bouet, L.; Glazov, M. M.; Amand, T.; Ivchenko, E. L.; Palleau, E.; Marie, X.; Urbaszek, B. Magneto-Optics in Transition Metal Diselenide Monolayers. *2D Mater.* **2015**, *2*, 034002.
(51) Tang, Y.; Mak, K. F.; Shan, J. Long Valley Lifetime of Dark Excitons in Single-Layer WSe_2. *arXiv Preprints* **2019**, arXiv:1903.12586.
(52) Hsu, W. T.; Chen, Y. L.; Chen, C. H.; Liu, P. S.; Hou, T. H.; Li, L. J.; Chang, W. H. Optically Initialized Robust Valley-Polarized Holes in Monolayer WSe_2. *Nat. Commun.* **2015**, *6*, 8963.
(53) Shi, L.; Hakala, T. K.; Rekola, H. T.; Martikainen, J. P.; Moerland, R. J.; Törmä, P. Spatial Coherence Properties of Organic Molecules Coupled to Plasmonic Surface Lattice Resonances in the Weak and Strong Coupling Regimes. *Phys. Rev. Lett.* **2014**, *112*, 153002.
(54) Sun, Z.; Gu, J.; Ghazaryan, A.; Shotan, Z.; Considine, C. R.; Dollar, M.; Chakraborty, B.; Liu, X.; Ghaemi, P.; Kéna-Cohen, S.; Menon, V. M. Optical Control of Room-Temperature Valley Polaritons. *Nat. Photonics* **2017**, *11*, 491−496.
(55) Galfsky, T.; Gu, J.; Narimanov, E. E.; Menon, V. M. Photonic Hypercrystals for Control of Light−Matter Interactions. *Proc. Natl. Acad. Sci. U. S. A.* **2017**, *114*, 5125−5129.
(56) Brotons-Gisbert, M.; Proux, R.; Picard, R.; Andres-Penares, D.; Branny, A.; Molina-Sánchez, A.; Sánchez-Royo, J. F.; Gerardot, B. D. Out-of-Plane Orientation of Luminescent Excitons in Atomically Thin Indium Selenide Flakes. *arXiv Preprints* **2019**, arXiv:1901.06719.
(57) Pifferi, A.; Torricelli, A.; Spinelli, L.; Contini, D.; Cubeddu, R.; Martelli, F.; Zaccanti, G.; Tosi, A.; Dalla Mora, A.; Zappa, F.; Cova, S. Time-Resolved Diffuse Reflectance Using Small Source-Detector Separation and Fast Single-Photon Gating. *Phys. Rev. Lett.* **2008**, *100*, 138101.
(58) Zhu, H.; Yi, J.; Li, M. Y.; Xiao, J.; Zhang, L.; Yang, C. W.; Kaindl, R. A.; Li, L. J.; Wang, Y.; Zhang, X. Observation of Chiral Phonons. *Science* **2018**, *359*, 579−582.
(59) Jin, C.; Ma, E. Y.; Karni, O.; Regan, E. C.; Wang, F.; Heinz, T. F. Ultrafast Dynamics in van Der Waals Heterostructures. *Nat. Nanotechnol.* **2018**, *13*, 994−1003.
(60) Rosker, M. J.; Dantus, M.; Zewail, A. H. Femtosecond Real-Time Probing of Reactions. I. The Technique. *J. Chem. Phys.* **1988**, *89*, 6113−6127.
(61) Huang, B.; Clark, G.; Klein, D. R.; MacNeill, D.; Navarro-Moratalla, E.; Seyler, K. L.; Wilson, N.; McGuire, M. A.; Cobden, D. H.; Xiao, D.; Yao, W.; Jarillo-Herrero, P.; Xu, X. Electrical Control of 2D Magnetism in Bilayer CrI_3. *Nat. Nanotechnol.* **2018**, *13*, 544−548.
(62) Zhao, C.; Norden, T.; Zhang, P.; Zhao, P.; Cheng, Y.; Sun, F.; Parry, J. P.; Taheri, P.; Wang, J.; Yang, Y.; Scrace, T.; Kang, K.; Yang, S.; Miao, G.; Sabirianov, R.; Kioseoglou, G.; Huang, W.; Petrou, A.; Zeng, H. Enhanced Valley Splitting in Monolayer WSe_2 Due to Magnetic Exchange Field. *Nat. Nanotechnol.* **2017**, *12*, 757−762.

DOI: 10.1021/acs.nanolett.9b02132
Nano Lett. 2019, 19, 6886−6893